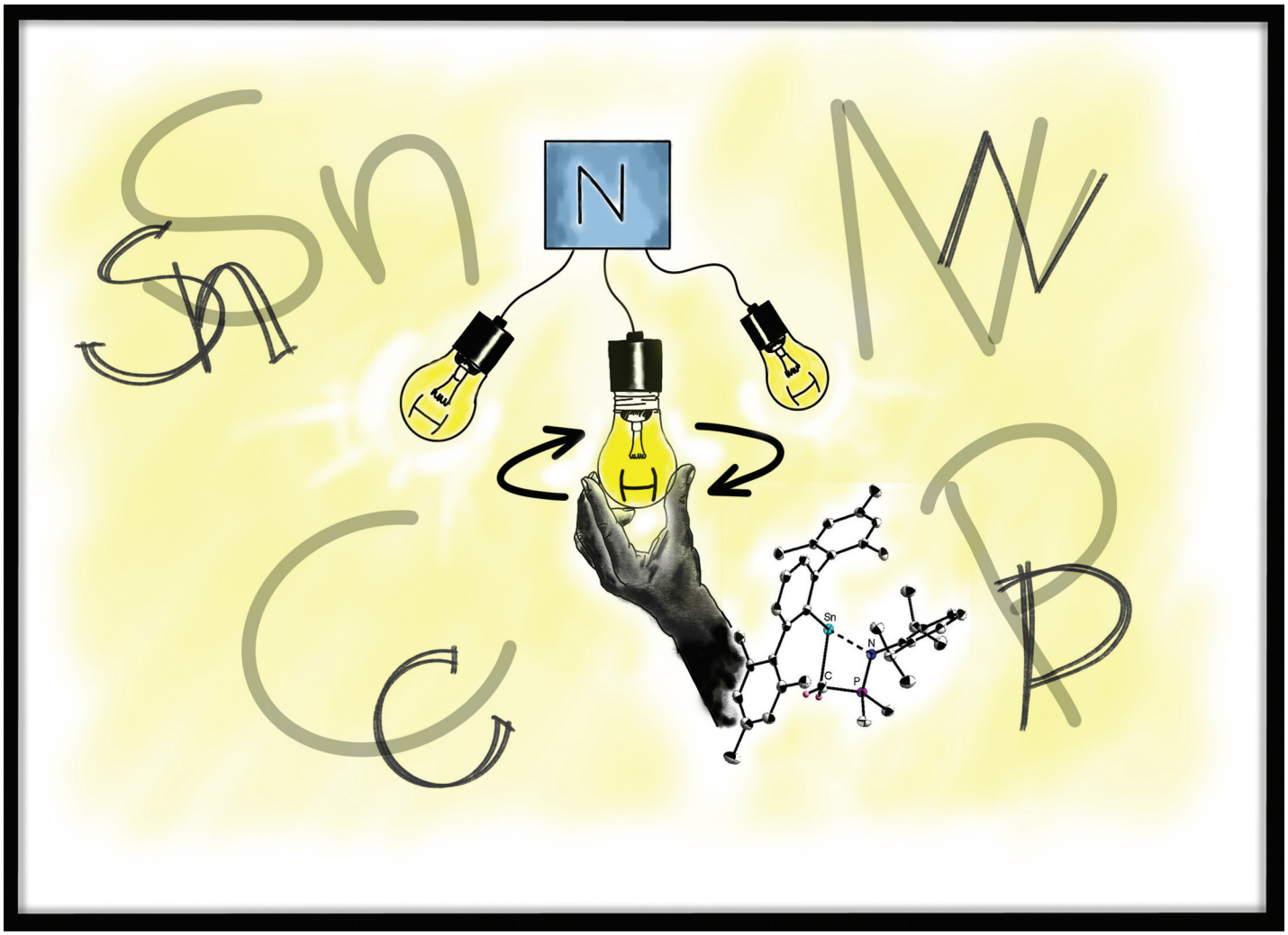

Showcasing research from Professor Fischer's laboratory, Institut für Anorganische Chemie, Georg-August-Universität Göttingen, D-37077, Germany.

Ammonia activation using a heteroleptic stannylene and lithium stannylenoid formation facilitated by hemilabile iminophosphorane-based ligands

Heteroleptic stannylenes featuring hemilabile iminophosphorane moieties and terphenyl ligands were synthesized and effectively employed for ammonia activation *via* N–H bond cleavage, uncovering an oxidation-state-independent activation pathway at tin. This study also revealed a novel route to a lithium stannylenoid.

As featured in:

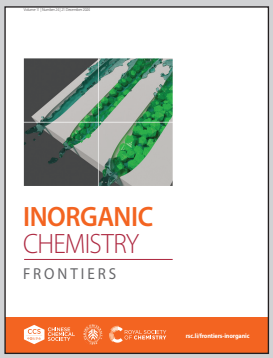

See Oliver P. E. Townrow, Malte Fischer *et al.*, *Inorg. Chem. Front.*, 2024, **11**, 8649.

CCS 中国化学会 CHINESE CHEMICAL SOCIETY
PEKING UNIVERSITY 1898
ROYAL SOCIETY OF CHEMISTRY
rsc.li/frontiers-inorganic

INORGANIC CHEMISTRY FRONTIERS

RESEARCH ARTICLE

View Article Online
View Journal | View Issue

Cite this: *Inorg. Chem. Front.*, 2024, **11**, 8649

Ammonia activation using a heteroleptic stannylene and lithium stannylenoid formation facilitated by hemilabile iminophosphorane-based ligands†

David M. J. Krengel,[a] Nico Graw,[a] Regine Herbst-Irmer,[a] Dietmar Stalke,[a] Oliver P. E. Townrow *[b] and Malte Fischer *[a]

Received 30th August 2024,
Accepted 27th September 2024

DOI: 10.1039/d4qi02202e

rsc.li/frontiers-inorganic

Heteroleptic stannylenes, featuring pendant hemilabile iminophosphorane functionalities and kinetically stabilizing terphenyl ligands, were synthesized straightforwardly through formal C–H activation. Subsequently, they were investigated for their ability to activate ammonia through N–H bond scission. By combining synthetic modifications of the ancillary ligand framework and computational analyses, detailed insights into the mechanism of NH_3 activation by these systems were obtained, highlighting an activation pathway at tin without a change in oxidation state. Additionally, an observed by-product during these studies underscores the non-innocence of a lithium salt in the synthesis of the stannylene starting materials, providing access to a novel lithium stannylenoid.

Introduction

The activation of small molecules like ammonia (NH_3) to construct complex nitrogen-containing value-added products is a significant and dynamic area of study, particularly considering both their widespread use as feedstocks due to large-scale synthesis in industrial processes and that a majority of homogeneous catalytic processes involves these molecules.[1] In this context, the direct hydroamination of non-activated alkenes with NH_3 has emerged as one of the 'holy grails' in catalysis.[2] Whilst transition metal complexes have traditionally been the focus of small molecule activation and catalysis, they face challenges in activating the N–H bond of ammonia, which has a high gas-phase bond dissociation energy of over 99 kcal mol^{-1}, and tend to form robust Werner type complexes.[3] In this context, the selective formation of monomeric transition metal amido hydride complexes through the oxidative addition of NH_3 has only been accomplished using two iridium-based pincer derivatives.[4] Main group species are increasingly gaining traction in this field, following the groundbreaking discoveries of NH_3 activation by cyclic (alkyl)(amino)carbenes (Scheme 1, **I**) and heavier alkyne analogues (Scheme 1, **III**).[5–7] More recently, advancements in NH_3 activation by main group compounds include thermoneutral and reversible ammonia splitting protocols using geometrically constrained phosphines,[8] activation *via* single-electron transfer protocols employing either a carbene-stabilized dithiolene zwitterion or a bismuth(II) complex,[9,10] and the pioneering report on catalytic NH_3 activation and transfer by an aluminium–carbon-

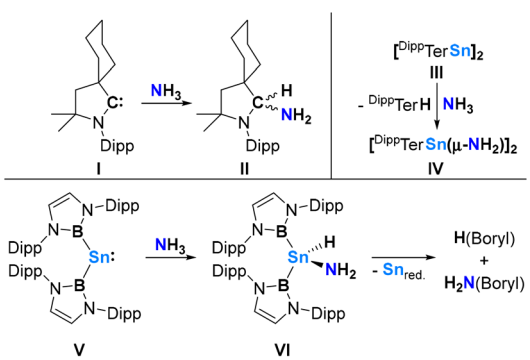

Scheme 1 Top: First reports on ammonia activation by Group 14 compounds **I** and **III**; bottom: Oxidative addition and reductive elimination sequence of ammonia by a bis(boryl)stannylene **V** (Dipp = 2,6-^{i}Pr-C_6H_3; ^{Dipp}Ter = 2,6-(2,6-^{i}Pr-C_6H_3)$_2$$C_6H_3$).

[a]*Institut für Anorganische Chemie, Georg-August-Universität Göttingen, Tammannstraße 4, D-37077 Göttingen, Germany. E-mail: malte.fischer@uni-goettingen.de*
[b]*Inorganic and Organometallic Chemistry, Friedrich-Alexander-Universität Erlangen-Nürnberg, Egerlandstraße 1, D-91058 Erlangen, Germany. E-mail: oliver.townrow@fau.de*

†Electronic supplementary information (ESI) available: Synthetic procedures, spectroscopic data, computational and crystallographic details. CCDC 2356897 (**2a**), 2356898 (**2c**), 2356899 (**3a**), 2356900 (**3c**), 2356901 (**4a**) and 2356902 (**7**). For ESI and crystallographic data in CIF or other electronic format see DOI: https://doi.org/10.1039/d4qi02202e

based ambiphile.[11] While a considerable number of Group 14-based systems (Si, Ge, Sn) have been developed to activate the N–H bond of ammonia,[5,6,12–14] further advancements are required to achieve the catalytic functionalization of unsaturated substrates by these systems. Thus, it is crucial to maintain a delicate balance in transferring the activated small molecule to a substrate while preserving the ability to activate the next small molecule (*i.e.* to form a catalytic cycle).

Given this consideration, heavier low-valent Group 14 compounds such as stannylenes show great promise due to their inherently weak M–E bonds (M = heavier tetrel element; E = H, N) and an accessible Sn^{II}/Sn^{IV} redox couple. However, only one example of oxidative addition of NH_3 by a stannylene (**V**) has been reported, capitalizing on strongly σ-donating boryl ligands (Scheme 1, **V**).[14] Decomposition from the Sn^{IV} intermediate **VI** to *N*-borylated products and reduced tin clusters indicates that further development in ligand design must be explored to tackle the challenge of instability and aggregation of the corresponding complexes after substrate activation. This is especially true for the heavier tetrel elements, such as tin, for which the low-valent form and, consequently, the +II oxidation state are thermodynamically favoured.

In this study, we introduce a direct synthetic approach for a range of stannylenes, bolstered by ancillary hemilabile[15] iminophosphorane ligands *via* an intermolecular C–H activation pathway. This strategy was designed to streamline activation processes at Sn^{II}, meanwhile furnishing a comprehensive mechanistic account of subsequent NH_3 activation within these frameworks. Furthermore, we have devised a straightforward protocol for the preparation of a lithium stannylenoid. Initially detected as a by-product during the synthesis of heteroleptic stannylenes featuring pendant iminophosphorane functionalities, this method offers a reliable route to its controlled synthesis.

Results and discussion

Synthesis and characterisation of heteroleptic stannylenes with pendant iminophosphorane functionalities

Reactions of the heteroleptic terphenyl-/amido stannylene $^{Mes}TerSn\{N(SiMe_3)_2\}$ (^{Mes}Ter = 2,6-(2,4,6-CH_3-C_6H_2)$_2$$C_6H_3$) (**1**) with freshly prepared imino-phosphoranes Me_3PNR (R = 2,6-$^{i}PrC_6H_3$ (Dipp) (**2a**), R = 3,5-$CH_3C_6H_3$ (Xyl) (**2b**), R = 1-adamantyl (Ad) (**2c**))[16] in C_6D_6 at room temperature lead to the formation of bis(trimethylsilyl)amine ($HN(SiMe_3)_2$), as evident from its characteristic ^{1}H NMR chemical shift (δ^1H = 0.10 ppm), and overall clean formation of the base-stabilized stannylenes $^{Mes}TerSnCH_2PMe_2NR$ (**3a–c**), each of which featuring a four-membered *Sn*,*C*,*P*,*N* heterocycle (Scheme 2A).

The formation of **3a–c** can be straightforwardly monitored by ^{31}P NMR spectroscopy, which shows the formation of new singlet signals with tin satellites. These signals are shifted to lower-field when compared to the iminophosphoranes **2a–c** (for an overview of characteristic NMR data of **2a–c** and **3a–c**, see Table 1).

Notably, whilst conversion to **3b** and **3c** is quantitative within hours at room temperature, the formation of **3a** is significantly slower. This can be mitigated by performing the reaction at 70 °C, leading to completion within 16 h. Overall, the multinuclear NMR spectroscopic data imply identical structures in solution, however, the Dipp-substituted derivative **3a** shows signal broadening at room temperature and the ^{119}Sn signal is low-field shifted, in comparison to **3b** and **3c**, by over 200 ppm.

The mechanisms for the formation of **3a–c** were investigated using Density Functional Theory (DFT) at the BP86-D3BJ/Def2-TZVP/Benzene(PCM) level of theory (Scheme 2C), finding that in all cases the reactions are exergonic (ΔG_{298K}: **3a**, −2.8 kcal mol^{-1}; **3b**, −10.0 kcal mol^{-1}; **3c** −10.1 kcal mol^{-1}; Scheme 2C). Comparison of the transition states ($\Delta G^{\ddagger}_{298K}$: **3a**, +31.6 kcal mol^{-1}; **3b**, +17.1 kcal mol^{-1}; **3c**, +19.1 kcal mol^{-1}) demonstrates the effect of higher steric bulk in **2a**, where steric restriction prohibits the formation of a stabilizing Sn–N interaction, resulting in a higher activation energy when compared to **2b** and **2c**. This correlates with the experimental findings, where heating is required to obtain a similar rate of reaction for the formation of **3a**, but not **3b** and **3c** (*vide supra*).

To elucidate any fluctional behaviour on the NMR timescale, a variable-temperature (VT) ^{1}H NMR (600 MHz) experiment of compound **3a** in toluene-d_8 was performed (Fig. S20†), showing that the signals with the best resolution are observed at 243 K (Fig. S23†).[17] At that temperature, the same signal pattern as for **3b** and **3c** is observed (*e.g.*, one signal each for the –CH_2PMe_2– moiety, three signals for the terphenyl methyl groups *etc.*). In the temperature range 193–353 K, the respective $^{31}P\{^1H\}$ and $^{119}Sn\{^1H\}$ NMR signals shift by $\Delta\delta^{31}P\{^1H\}$ = 4.7 and $\Delta\delta^{119}Sn\{^1H\}$ = 49.2 ppm, respectively. This leads to the assumption that in solution more pronounced dative interactions between the nitrogen functionalities and the tin atoms in **3b,c** when compared to **3a** are responsible for the high-field shift in the $^{119}Sn\{^1H\}$ NMR spectra. Notably, compared to true two-coordinate stannylenes, the observed $^{119}Sn\{^1H\}$ NMR chemical shifts of **3a–c** are significantly shifted upfield. For instance, the starting material **1** exhibits a $^{119}Sn\{^1H\}$ NMR chemical shift of $\delta^{119}Sn\{^1H\}$ = 1192.3 ppm (Fig. S83†).[17]

3a–c were purified by crystallization from aliphatic hydrocarbons and in the case of **3a** and **3c**, crystalline material suitable for single crystal X-ray diffraction (SCXRD) analysis was obtained, with the molecular structure of **3a** being shown in Scheme 2B.[17] The dative interaction between Sn1–N1 is suggested by relatively long distances (2.2877(14) Å (**3a**) and 2.269(2) Å (**3c**)), both significantly exceeding the respective single bond radii of the respective atoms (2.11 Å) by at least 0.15 Å.[18] This dative interaction and the formation of respective four-membered *Sn*,*C*,*P*,*N* rings is further supported by almost perpendicular Sn1–C25–P1 angles of 91.90(7)° (**3a**) and 91.86(9)° (**3c**), respectively. By comparing the structures of the herein obtained free iminophosphoranes **2a,c** with **3a,c**, the respective nitrogen–phosphorus bond lengths are elongated by approximately 0.06 Å (1.6143(13) Å (**3a**) and 1.6116(17) Å (**3c**) *vs.* 1.5569(17) Å (**2a**) and 1.558(4) Å (**2c**)[19]), indicative of

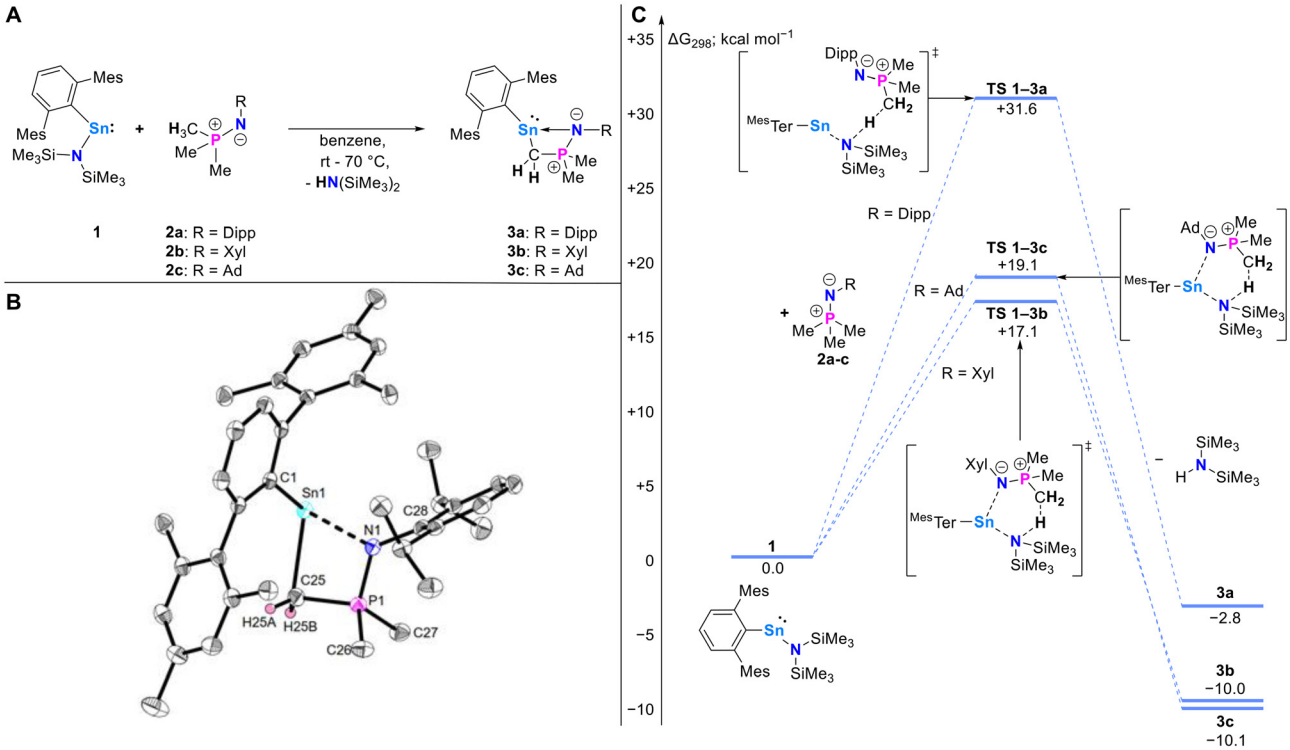

Scheme 2 (A) Reactivity of stannylene **1** towards iminophosphoranes **2a–c** to give stannylenes **3a–c**. (B) Molecular structure of ^{Mes}TerSnCH$_2$PMe$_2$NDipp (**3a**) determined by single crystal X-ray crystallography. Anisotropic displacement parameters are drawn at the 50% probability level (hydrogen atoms (except for H25A and H25B) and lattice solvent have been omitted for clarity). Selected bond lengths (Å) and angles (°): Sn1···N1 2.2877(14), Sn1–C1 2.2527(16), Sn1–C25 2.3220(17), P1–N1 1.6143(13), P1–C25 1.7503(17), P1–C26 1.8001(17), P1–C27 1.8050(17), N1–C28 1.426(2), C1–Sn1–C25 106.05(6), P1–C25–Sn1 91.90(7), C25–P1–N1 100.92(7), P1–N1–C28 127.42(11). (C) Computed mechanism for the formation of **3a–c** from **1** and **2a–c** (BP86-D3BJ/Def2-TZVP/Benzene(PCM)).

Table 1 Selected characteristic NMR data of **2a–c** and **3a–c**[a]

Compound	δ^{31}P, $J_{119/117Sn,P}$[c]	δ ^{119}Sn, $^2J_{Sn,P}$	δ ^{1}H(PCH$_2$)	δ ^{1}H(P(CH$_3$)$_n$)[b]
2a	−8.2	—	—	0.93
2b	1.4	—	—	0.95
2c	−14.5	—	—	1.00
3a	40.4 $J_{119/117Sn,P}$ = 163.6	422.0 $^2J_{Sn,P}$ = 165.9	0.24	0.72
3a[d]	—	—	0.14 and 0.28	0.58
3b	42.1 $J_{119/117Sn,P}$ = 142.3	217.6 $^2J_{Sn,P}$ = 145.7	0.39 and 0.47	0.63 and 1.00
3c	33.8 $J_{119/117Sn,P}$ = 137.6	213.3 $^2J_{Sn,P}$ = 138.6	0.39 and 0.62	0.62 and 0.74

[a] δ values are given in ppm and J values in Hz. The data is given in benzene-d_6 as solvent and at room temperature. [b] n = 3 for **2a–c** and n = 2 for **3a–c**. [c] Average value given. [d] The data is given in toluene-d_8 as solvent and at 243 K.

reduced charge transfer from the nitrogen atom to phosphorus but increased to the tin atom.[20] The structural data is in good agreement to a previously reported five-membered *Sn,C,C,P,N* complex which was obtained through the reaction of the respective Sn–P Lewis pair with an organic azide (N–P 1.613(5)/1.608(4) Å; Sn–N 2.305(4)/2.292(4) Å).[21]

To obtain insights into the bonding within the core of **3a–c**, DFT and Natural Bond Orbital (NBO) calculations were performed.

Inspection of the Kohn–Sham frontier molecular orbitals of **3a–c** shows major contribution from the tin atomic orbitals, with a lone pair of electrons and orthogonal p-orbital in the HOMO and LUMO respectively (Fig. S84–S86†), which is typical for divalent Group 14 atoms.[17] Further analysis of the Lewis structure by NBO 7.0[22] reveals a lone pair of electrons ($s^{0.88}p^{0.12}$ hybridised, 1.95 e$^-$) in addition to two covalent, polar Sn–C single bonds around the tin atom (polarised 78% and 83% towards C), with no NBO describing a covalent Sn–N

interaction, as expected from the elongated Sn···N interatomic distances found in the crystal structures (Fig. S89–S91†).[17] Second Order Perturbation Theory analysis revealed a significant donor–acceptor interaction between the Sn and N atoms, with the nitrogen lone pair (LP) datively bonding into a valence lone vacant (LV) orbital at Sn with an energy of 40.7 kcal mol^{-1}. This energy increases to 53.2 and 49.8 kcal mol^{-1} when the less sterically demanding xylyl or adamantyl substituents are present in **3b** and **3c**, respectively, aligning well with the observations from ^{119}Sn NMR spectroscopy. In addition, the phosphorus bears four single bonds to each of its surrounding carbon and nitrogen neighbours, in line with the description of a zwitterionic $^{-}$N–P^{+} moiety. The drain of N-charge density to the tin atom causes an elongation of the P–N bonds in comparison to the parent iminophosphoranes **2a–c**.

Based on both the crystallographic and theoretical insights, it is most appropriate to describe this ligand moiety as zwitterionic, bonding covalently only *via* the carbon atom.[20]

Investigations on hemilability of the iminophosphorane-based ligand

To investigate the potential replacement of the nitrogen donor functionality with stronger Lewis bases and experimentally probe the hemilability of the selected ligand framework, we examined the reactivity of **3a–c** towards the *N*-heterocyclic carbene (NHC) 1,3,4,5-tetramethyl-2-imidazol-2-ylidene (IMe$_4$). Accompanied by subtle yet noticeable colour changes in the reaction mixtures, we observed the clean formation of the corresponding NHC-stabilized stannylenes ^{Mes}TerSn(IMe$_4$)CH$_2$PMe$_2$NR (**4a–c**) (Scheme 3A). Due to the coordination of the NHC to the tin atoms in **4a–c**, the ^{31}P and ^{119}Sn resonances are observed at higher field (*e.g.*, δ^{31}P{^{1}H} = 5.6 ppm; δ^{119}Sn{^{1}H} = −175.1 ppm for **4a**; *cf.* Table 1).

The molecular structure was verified crystallographically in **4a** (Scheme 3B), revealing no tin–nitrogen donor–acceptor interaction (Sn1···N1 > 3.5 Å). The tin–carbene separation (Sn1–C40 2.287(3) Å) aligns with that observed in other stannylene carbene adducts.[16] Consequently, the P1–N1 bond length of 1.573(3) Å in **4a** is shorter than that observed in starting material **3a** (1.6143(13) Å). The maintained electron density at the nitrogen atom now reinforces the P$^{\delta+}$–N$^{\delta-}$ bond to almost the value in the free iminophosphorane **2a** (1.5569(17) Å).

The electronic structure of the 3-coordinate tin compound **4a** was investigated by NBO analysis, revealing a lone pair of electrons (s$^{0.81}$p$^{0.19}$ hybridized, 1.93 e^{-}) situated at the Sn^{II} atom, in addition to three polar, covalent Sn–C single bonds (Fig. S92†). The IMe$_4$ moiety adopts the imidazolium resonance form, characterized by one bonding (BD) NBO describing an external Sn–C σ-bond. NBO analysis further gives a 3-center-4-electron hyperbond between N97, C93, and N94 (across the NCN interface of the NHC), combining two NBOs (shown In Fig. S92†) in a ratio of 49.3 to 50.7 and a total electron count of 3.86.

In addition, as in the case of **3**, the P–N functionality is zwitterionic, with the phosphorus atom forming four single bonds to each of its surrounding bonding partners, characterized by four bonding NBOs.

Ammonia activation with 3a–c

Comparison of the singlet–triplet energy difference and the magnitude of the HOMO–LUMO gap of divalent Group 14 atoms has been shown to be indicative for the tendency of such systems to undergo E–H oxidative addition (E = H, NR$_2$, OR).[23] Furthermore, considering the kinetics of E–H oxidative addition, it has been reported that the energy gap between the metallylene singlet ground state and the triplet excited state is inversely correlated with reactivity.[23] Additionally, σ-donating substituents based on electropositive elements, in relation to the heavier tetrel elements, such as carbon, silicon, and boron have been demonstrated to reduce the HOMO–LUMO gap through destabilization of the HOMO.[6,14,23,24] The boryl-substituted stannylene **V** and its NH$_3$ adduct reported by Aldridge

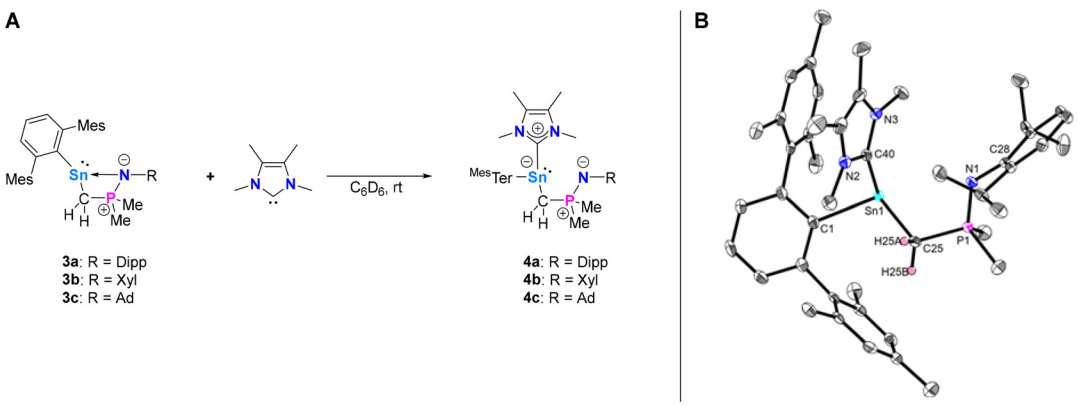

Scheme 3 (A) Reactivity of **3a–c** towards IMe$_4$ to give the NHC-stabilized stannylenes **4a–c**. (B) Molecular structure of ^{Mes}TerSn(IMe$_4$)CH$_2$PMe$_2$NDipp (**4a**) determined by single crystal X-ray crystallography. Anisotropic displacement parameters are drawn at the 50% probability level (hydrogen atoms, except for H25A and H25B, and second molecule have been omitted for clarity). Selected bond lengths (Å) and angles (°): Sn1···N1 3.571(3), Sn1–C1 2.269(3), Sn1–C25 2.263(3), Sn1–C40 2.287(3), N1–P1 1.573(3), P1–C25 1.766(3), C1–Sn1–C25 104.09(12), C1–Sn1–C40 92.65(11), C25–Sn1–C40 90.49(11).

et al.,[14] which enables the N–H oxidative addition of ammonia, has a DFT calculated singlet–triplet difference and HOMO–LUMO gap of −11.45 kcal mol^{-1} and −1.12 eV respectively (recalculated at the BP86-D3BJ/def2-TZVP level of theory to align with our methodology). **3a–c**, on the other hand, bear carbon-based ligands, and possess comparatively large singlet–triplet energy differences and HOMO–LUMO gaps (**3a**: −35.0 kcal mol^{-1}, +2.67 eV; **3b**: −34.0 kcal mol^{-1}, +2.98 eV; **3c**: −41.7 kcal mol^{-1}, +2.97 eV) (Fig. S84–S86†).[17] This renders the oxidative addition of E–H-containing substrates such as ammonia a challenging task with these systems.

We hypothesized however, that the pendant, hemilabile, iminophosphorane-based ligand might facilitate ammonia activation by combining a hydrogen bonding $N_{ammonia}$–H···N_{Ligand} interaction and a donor–acceptor $N_{ammonia}$ → Sn interaction to form a six-membered transition state. This would thus allow for the oxidation-state-neutral NH_3 activation with respect to the tin ambiphile.

Accordingly, **3a–c** were reacted with 1.2 bar NH_3 in C_6D_6 at room temperature (Scheme 4A). To our delight, clean reactions were observed by immediately monitoring the reaction progress using ^{1}H and ^{31}P NMR spectroscopy. Interestingly, these reactions varied depending on the substitution pattern at nitrogen. The Ad-substituted derivative **3c** reacts cleanly within 30 minutes, and the formation of the free iminophosphorane **2c** was observed by its characteristic ^{31}P NMR chemical shift at δ^{31}P = −14.5 ppm, with no detectable intermediates (Fig. S71†).[17] In contrast, the reaction of the Xyl-substituted derivative **3b** results in the consumption of the starting material and the observed signal broadening of the ^{31}P NMR signal corresponding to **3b** over the course of 24 hours at room temperature, leading to the formation of iminophosphorane **2b** (Fig. S69†).[17] The Dipp-substituted derivative **3a**, under the same reaction conditions, exhibits a broad ^{31}P resonance at δ^{31}P = 16.3 ppm in addition to the observed ^{31}P NMR signal resembling the free iminophosphorane **2a**, which gradually

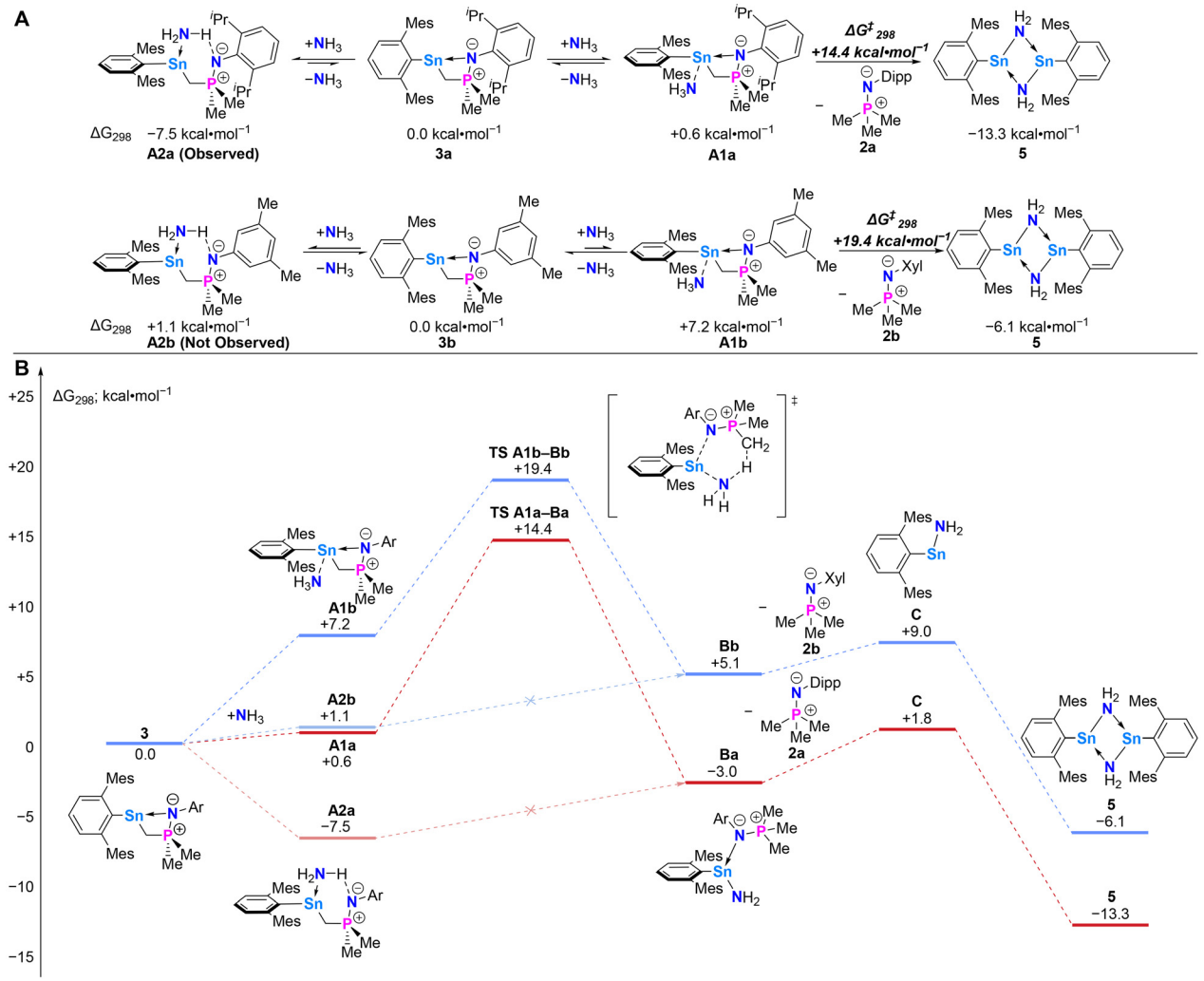

Scheme 4 Mechanistic investigation of ammonia activation at complexes **3a** and **3b**. (A) Reactivity of **3a**,**b** towards ammonia to give the bridged tin amide [^{Mes}TerSn(μ-NH_2)]$_2$ (**5**) and free iminophosphoranes **2a**,**b**. (B) Calculated mechanisms (BP86-D3BJ/def2-TZVP) for the formation of **5** from **3a** (red) or **3b** (blue); An energy difference of 7.2 kcal mol^{-1} is an effect of the different Ar group used.

decreased over approximately 16 hours to yield **2a** as the sole P-containing species (Fig. S70†).[17] In all cases, the tin containing product was identified to be the literature-known NH_2 bridged dimer [^{Mes}TerSn(μ-NH_2)]$_2$ (**5**) as verified by SCXRD and multinuclear NMR spectroscopy (Scheme 4A and Fig. S73–S75†).[17,25]

To test our initial hypothesis and gain insight into the mechanism for the N–H activation of ammonia by aryl-substituted **3a** and **3b**, DFT investigations were conducted (Scheme 4B). Contrary to their formation, they were found to be almost identical. Two barrierless pathways were found for the approach of NH_3 towards Sn, resulting in two different encounter complexes as possible intermediates (**A**). Whilst the intermediate **A2**, which features an intramolecular hydrogen bond, was found to be the energetically most favourable of the two (ΔG_{298}: −7.5 kcal mol^{-1}; +1.1 kcal mol^{-1}), no pathway towards a lower energy activation product was found, and so it is most likely in equilibrium with the starting materials. This reflects the experimental data, where an intermediate with ^{1}H and ^{31}P NMR signals consistent with an ammonia complex is initially observed for **3a** + NH_3, whereas in the case of **3b** + NH_3, only some signal broadening can be seen.

Following the barrierless formation of encounter complex **A1** (ΔG_{298}: +0.6 kcal mol^{-1}; +7.2 kcal mol^{-1}) however, the ammonia N–H can then undergo metathesis across the Sn–C bond ($\Delta G^{\ddagger}_{298}$ +14.4 kcal mol^{-1}; +19.4 kcal mol^{-1}), in a similar concerted transition state to that in the formation of **3b** (Scheme 2C) and its cooperative nature is also reminiscent of that found recently for the N–H metathesis of ammonia across a P–N bond.[26]

This produces the base-stabilized terphenyl Sn^{II} amido intermediate **B** (ΔG_{298}: −3.0 kcal mol^{-1}; +5.1 kcal mol^{-1}) which undergoes a barrierless disassociation of **2**, to form intermediate **C** (ΔG_{298}: +1.8 kcal mol^{-1}; +9.0 kcal mol^{-1}), which finally dimerises to the crystallographically and NMR spectroscopically characterized **5**, thus providing the thermodynamic driving force for the overall reaction (ΔG_{298} −13.3 kcal mol^{-1}; −6.1 kcal mol^{-1}). Due to the observed formation of an intermediate during the reaction of **3a** with NH_3 and to evidence our hypothesis of ammonia–adduct formation, a sample of **3a** in toluene-d_8 was reacted with 1.2 bar of NH_3 whilst keeping the sample at low temperature (−80 °C) for its *in situ* characterization by multinuclear NMR spectroscopy.[17] Indeed, the corresponding ammonia adduct ^{Mes}TerSn(NH_3)CH_2PMe_2NDipp (**A2a**) was successfully identified, and the observed signal pattern perfectly matched those of the stannylene–carbene adducts **4a–c** reported in this study (Scheme 5).[17] It is noteworthy that **4a–c** did not react with ammonia even under harsher conditions (2 bar NH_3, prolonged heating up to 100 °C), likely due to the strong coordination of the NHC to the tin atom, persistently blocking Lewis base coordination of NH_3.

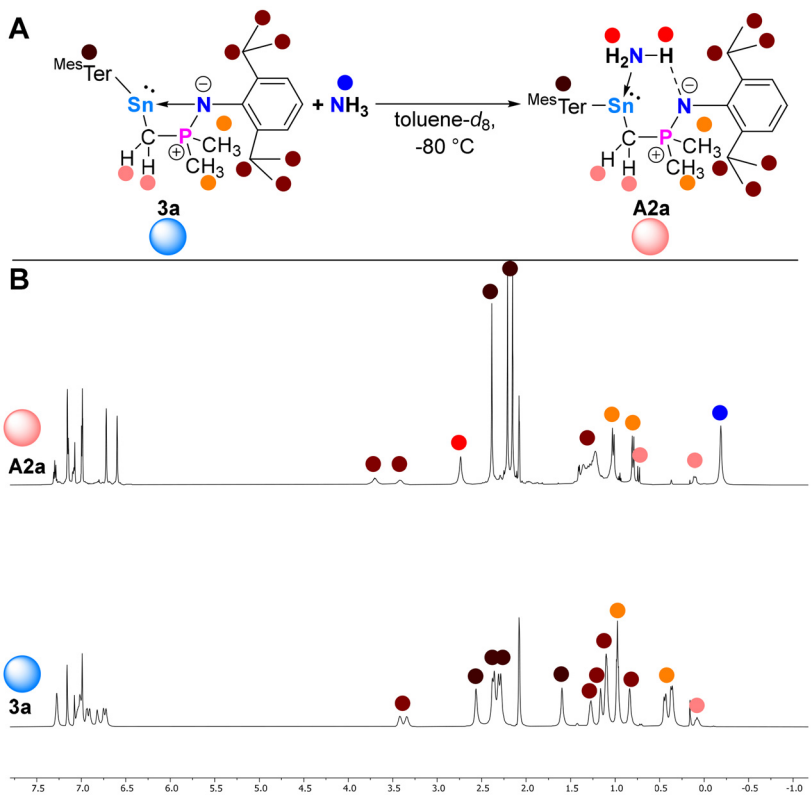

Scheme 5 A: Synthesis of intermediate **A2a** at −80 °C in toluene-d_8; B: Stacked ^{1}H NMR spectra of **3a** and **A2a** at −80 °C in toluene-d_8.

Synthesis and characterization of the lithium stannylenoid 7

During the investigations of ammonia activation by **3a**, a by-product (**7**) (up to 10%) was occasionally detected by ^{31}P NMR spectroscopy at a chemical shift of δ^{31}P = 30.5 ppm during its synthesis. We found that this occurred when **3a–c** were synthesized from dried mother liquors of **1**, rather than crystalline material, presumable due to small amounts of lithium bis(trimethylsilyl)amide (LiN(SiMe$_3$)$_2$) being carried through from its synthesis (Sn{N(SiMe$_3$)$_2$}$_2$ + ^{Mes}TerLi) reacting with **2a**, generating a reactive intermediate.[16]

To confirm this experimentally, we targeted independent synthetic routes to synthesize **7**.

By reacting **2a** with equimolar amounts of LiN(SiMe$_3$)$_2$ in benzene, complete consumption of **2a** was observed, resulting in the formation of apparently two new species in a 3 : 1 ratio according to ^{31}P NMR spectroscopy: one broad singlet at δ^{31}P = 11.3 ppm and one sharp singlet at δ^{31}P = 25.9 ppm. Through analysis of the multinuclear NMR data and employing ECC-DOSY NMR spectroscopy (with adamantane as the internal standard), we identified the minor component of the product mixture as the lithium salt "LiCH$_2$PMe$_2$NDipp" (**6**).[17,27,28] Despite its heterogeneity, this mixture could still serve as a readily accessible source of "LiCH$_2$PMe$_2$NDipp" (**6**) for the synthesis of compound **7**.

By either reacting **1** with two equivalents of **6** or reacting **3a** with one equivalent of the **6**, clean conversions towards the species with the phosphorus resonance at δ^{31}P = 30.5 ppm are observed (see Scheme 6A).

Recrystallization from *n*-hexane at −30 °C clearly confirms the compound to be the lithium stannylenoid (lithium stannate(II)) [^{Mes}TerSn(CH$_2$PMe$_2$NDipp)]$_2$Li (**7**), which was isolated as a colourless crystalline material (see Scheme 6B).

The molecular structure of **7** reveals the tin atom to be three-coordinate (Σ∢Sn = 298.4(3)°), with all tin–carbon bond lengths (Sn1–C1 2.242(3) Å, Sn1–C25 2.293(3) Å, Sn1–C28 2.288(3) Å) falling within the same range, typical of tin–carbon single bonds (single bond covalent radii: 2.15 Å (ref. 18)), and in good agreement with the molecular structures of **3a,c**, and **4a** reported herein. NBO analysis found a lone pair of electrons situated at the Sn^{II} atom (s$^{0.81}$p$^{0.19}$ hybridized, 1.91e$^-$), in addition to three polar, covalent tin–carbon single bonds (Fig. S93†).[17] The interatomic distances P1–N1 1.598(2) Å and P2–N2 1.596(2) Å fall between those of **3a** and **4a**. Accordingly, **7** bears two zwitterionic iminophosphine arms, which have similar electronic structures to those described for **3a** (*vide supra*). The lithium–nitrogen bond lengths (mean value 1.923(6) Å) fall within the same range as observed for other lithium stannylenoids, *e.g.*, in the lithium bis(imino)stannylenoid ClSn(NIPr)$_2$Li (1.946(9) Å and 2.004(9) Å; NIPr = bis(2,6-(diisopropylphenyl)imidazolin-2-imino)).[29] A lone pair of electrons on each nitrogen atom directs towards the lithium cation situated in the centre; however, as expected, no significant donor–acceptor interaction was found by Second Order Perturbation Theory analysis. The Sn1···Li1 distance of 2.913(5) Å clearly exceeds the sum of covalent radii (2.73 Å (ref. 18)) and accordingly, no bonding interaction between the lithium and the tin atom is detected.[30]

The ^{119}Sn{^{1}H} NMR spectrum displays a doublet resonance for the trigonal pyramidal coordinated tin atom due to coupling to phosphorus ($^2J_{Sn,P}$ = 167.0 Hz) at δ^{119}Sn{^{1}H} = 437.9 ppm, placing it in the same range as observed for **3a** (Table 1). Additionally, a singlet is observed in the ^{7}Li{^{1}H} NMR spectrum at δ^7Li{^{1}H} = 1.3 ppm.

7 joins the ranks of scarce examples of structurally characterized and largely unexplored stannylenoids,[31] thus representing a heavier congener of a carbenoid.[32] Its synthesis has been proven to be straightforward, starting from the respective stannylenes **1** or **3a**, respectively.

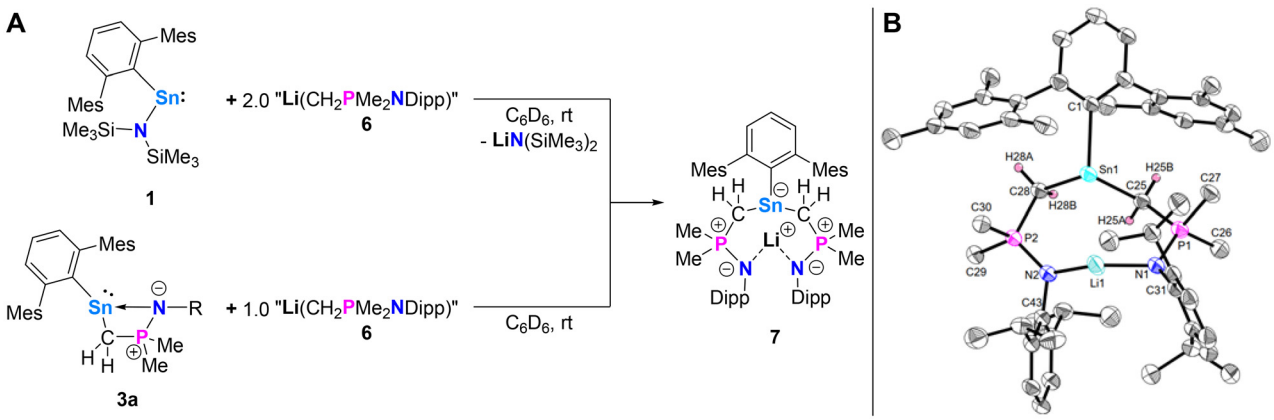

Scheme 6 (A) Synthesis of lithium stannylenoid **7**. (B) Molecular structure of ^{Mes}TerSn(CH$_2$PMe$_2$NDipp)$_2$Li (**7**) in the crystal. Anisotropic displacement parameters are drawn at the 50% probability level (hydrogen atoms, except for H25A, H25B, H28A and H28B, have been omitted for clarity). Selected bond lengths (Å) and angles (°): Sn1–C1 2.242(3), Sn1–C25 2.293(3), Sn1–C28 2.288(3), N1–P1 1.598(2), N2–P2 1.596(2), Sn1···Li1 2.913(5), Li1–N1 1.921(5), Li1–N2 1.924(6), P1–C25 1.766(3), P2–C28 1.773(3), P1–C26 1.822(3), P1–C27 1.800(3), P2–C29 1.807(3), P2–C30 1.804(3), N1–C31 1.429(4), N2–C43 1.428(3), C1–Sn1–C25 106.51(10), C1–Sn1–C28 100.13(10), C25–Sn1–C28 91.72(11), N1–P1–C25 108.65(13), N2–P2–C28 109.55 (13), N1–Li1–N2 147.1(3).

Conclusions

In conclusion, we present a comprehensive investigation into the activation of ammonia by heteroleptic stannylenes featuring pendant hemilabile *N*-donor iminophosphorane functionalities. These stannylenes are accessed *via* formal C–H activation at a C(sp^3)–H moiety adjacent to the phosphorus atom in the employed free iminophosphoranes in reactions with the heteroleptic amido-/terphenyl-stannylene precursor. Our findings reveal that these systems react with ammonia, cleaving one N–H bond in a redox-neutral manner, thus tin maintains in its +II oxidation state throughout the process. Depending on the *N*-substituent, spectroscopic characterization of an ammonia–stannylene adduct is possible, and the mechanism of ammonia activation is rationalized computationally. Furthermore, we discovered the non-innocence of lithium hexamethyldisilazide, originating from the synthesis of the stannylene starting materials, leading to the development of a straightforward synthetic protocol for a novel lithium stannylenoid.

Author contributions

D. M. J. K. and M. F. carried out the experimental work. N. G., R. H.-I., and D. S. were responsible for the SCXRD experiments. O. P. E. T. carried out the quantum chemical calculations and wrote the initial draft of the computational part of the manuscript. M. F. was responsible for the conceptualization, supervision of the experimental investigations, and wrote the initial draft of the manuscript. All authors contributed to the finalization of the manuscript and agreed to the submitted content.

Data availability

The data that support the findings of this study are available in the ESI† of this manuscript or by contacting the authors. Included are synthetic and characterizing data, representative spectra, details of the X-ray crystal structures and quantum chemical calculations. X-ray data is further available through the CCDC. The authors have cited additional references within the ESI.†[33–49]

Conflicts of interest

The authors declare no conflict of interest.

Acknowledgements

Financial support (VCI Liebig fellowship for M.F., Alexander von Humboldt post-doctoral fellowship for O.P.E.T.) is gratefully acknowledged. M. F. further wishes to acknowledge the Georg-August-Universität Göttingen for financial support and Prof. Inke Siewert for her continuous support and guidance. The research group led by Prof. Sven Schneider, with special mention to Marc Neben, Felix Fuchs and Sven Rosendahl, is warmly acknowledged for granting access to their ammonia line and for their assistance in its utilization. We thank Franziska Rüttger (research group led by Prof. Dietmar Stalke) for assistance with the interpretation of the DOSY NMR data.

References

1 J. F. Hartwig, *Organotransition Metal Chemistry: From Bonding to Catalysis*, University Science Books, Sausalito, CA, 2010.
2 S. Streiff and F. Jérôme, Hydroamination of non-activated alkenes with ammonia: a holy grail in catalysis, *Chem. Soc. Rev.*, 2021, **50**, 1512–1521.
3 M. J. Bezdek, S. Guo and P. J. Chirik, Coordination-induced weakening of ammonia, water, and hydrazine X–H bonds in a molybdenum complex, *Science*, 2016, **354**, 730–733.
4 (*a*) J. Zhao, A. S. Goldman and J. F. Hartwig, Oxidative Addition of Ammonia to Form a Stable Monomeric Amido Hydride Complex, *Science*, 2005, **307**, 1080–1082; (*b*) E. Morgan, D. F. MacLean, R. McDonald and L. Turculet, Rhodium and Iridium Amido Complexes Supported by Silyl Pincer Ligation: Ammonia N–H Bond Activation by a [PSiP]Ir Complex, *J. Am. Chem. Soc.*, 2009, **131**, 14234–14236.
5 G. D. Frey, V. Lavallo, B. Donnadieu, W. W. Schoeller and G. Bertrand, Facile splitting of hydrogen and ammonia by nucleophilic activation at a single carbon center, *Science*, 2007, **316**, 439–441.
6 Y. Peng, B. D. Ellis, X. Wang and P. P. Power, Diarylstannylene Activation of Hydrogen or Ammonia with Arene Elimination, *J. Am. Chem. Soc.*, 2008, **130**, 12268–12269.
7 (*a*) P. P. Power, Main-group elements as transition metals, *Nature*, 2010, **463**, 171–177; (*b*) S. Yadav, S. Saha and S. S. Sen, Compounds with Low-Valent p-Block Elements for Small Molecule Activation and Catalysis, *ChemCatChem*, 2016, **8**, 486–501; (*c*) C. Weetman and S. Inoue, The Road Travelled: After Main-Group Elements as Transition Metals, *ChemCatChem*, 2018, **10**, 4213–4228; (*d*) L. Greb, F. Ebner, Y. Ginzburg and L. M. Sigmund, Element-Ligand Cooperativity with p-Block Elements, *Eur. J. Inorg. Chem.*, 2020, 3030–3047; (*e*) J. Abbenseth and J. M. Goicoechea, Recent developments in the chemistry of non-trigonal pnictogen pincer compounds: from bonding to catalysis, *Chem. Sci.*, 2020, **11**, 9728–9740; (*f*) F. Hanusch, L. Groll and S. Inoue, Recent advances of group 14 dimetallenes and dimetallynes in bond activation and catalysis, *Chem. Sci.*, 2021, **12**, 2001–2015; (*g*) J. M. Lipshultz, G. Li and A. T. Radosevich, Main Group Redox Catalysis of Organopnictogens: Vertical Periodic Trends and Emerging Opportunities in Group 15, *J. Am. Chem. Soc.*, 2021, **143**, 1699–1721; (*h*) K. Oberdorf and C. Lichtenberg, Small

molecule activation by well-defined compounds of heavy p-block elements, *Chem. Commun.*, 2023, **59**, 8043–8058; (*i*) T. J. Hannah and S. S. Chitnis, Ligand-enforced geometric constraints and associated reactivity in p-block compounds, *Chem. Soc. Rev.*, 2024, **53**, 764–792.

8 (*a*) A. J. King and J. M. Goicoechea, Ligand Centered Reactivity of a Transition Metal Bound Geometrically Constrained Phosphine, *Chem. – Eur. J.*, 2024, **30**, e202400624For NH_3 activation with phosphorus-based compounds see also:(*b*) S. M. McCarthy, Y.-C. Lin, D. Devarajan, J. W. Chang, H. P. Yennawar, R. M. Rioux, D. H. Ess and A. T. Radosevich, Intermolecular N–H Oxidative Addition of Ammonia, Alkylamines, and Arylamines to a Planar σ^3-Phosphorus Compound via an Entropy-Controlled Electrophilic Mechanism, *J. Am. Chem. Soc.*, 2014, **136**, 4640–4650; (*c*) K. Cui, Y. Li, R. Ganguly, A. Inthirarajah, H. Hirao and R. Kinjo, Metal-Free σ-Bond Metathesis in Ammonia Activation by a Diazadiphosphapentalene, *J. Am. Chem. Soc.*, 2014, **136**, 16764–16767; (*d*) T. P. Robinson, D. M. De Rosa, S. Aldridge and J. M. Goicoechea, E–H Bond Activation of Ammonia and Water by a Geometrically Constrained Phosphorus(III) Compound, *Angew. Chem., Int. Ed.*, 2015, **54**, 13758–13763, (*Angew. Chem.*, 2015, **127**, 13962–13967); (*e*) A. Hinz, A. Schulz and A. Villinger, Metal-Free Activation of Hydrogen, Carbon Dioxide, and Ammonia by the Open-Shell Singlet Biradicaloid $[P(\mu\text{-NTer})]_2$, *Angew. Chem., Int. Ed.*, 2016, **55**, 12214–12218, (*Angew. Chem.*, 2016, **128**, 12402–12406); (*f*) R. Streubel, A. Schmer, A. W. Kyri and G. Schnakenburg, 1,1′-Bifunctional Aminophosphane Complexes via N–H Bond Insertions of a Li/Cl Phosphinidenoid Complex and First Studies on N/P Mono Functionalizations, *Organometallics*, 2017, **36**, 1488–1495; (*g*) S. Volodarsky and R. Dobrovetsky, Ambiphilic geometrically constrained phosphenium cation, *Chem. Commun.*, 2018, **54**, 6931–6934; (*h*) F. Dankert, J.-E. Siewert, P. Gupta, F. Weigend and C. Hering-Junghans, Metal-Free N–H Bond Activation by Phospha-Wittig-Reagents, *Angew. Chem., Int. Ed.*, 2022, **61**, e202207064, (*Angew. Chem.*, 2022, **134**, e202207064).

9 Y. Wang, P. M. Tran, M. E. Lahm, Y. Xie, P. Wie, E. R. Adams, J. N. Glushka, Z. Ren, V. V. Popik, H. F. Schaefer III and G. H. Robinson, Activation of Ammonia by a Carbene-Stabilized Dithiolene Zwitterion, *J. Am. Chem. Soc.*, 2022, **144**, 16325–16331.

10 X. Yang, E. J. Reijerse, K. Bhattacharyya, M. Leutzsch, M. Kochius, N. Nöthling, J. Busch, A. Schnegg, A. A. Auer and J. Cornella, Radical Activation of N–H and O–H Bonds at Bismuth(II), *J. Am. Chem. Soc.*, 2022, **144**, 16535–16544.

11 F. Krämer, J. Paradies, I. Fernández and F. Breher, A crystalline aluminium–carbon-based ambiphile capable of activation and catalytic transfer of ammonia in non-aqueous media, *Nat. Chem.*, 2024, **16**, 63–69.

12 Ammonia activation by selected Si compounds:(*a*) A. Jana, C. Schulzke and H. W. Roesky, Oxidative Addition of Ammonia at a Silicon(II) Center and an Unprecedented Hydrogenation Reaction of Compounds with Low-Valent Group 14 Elements Using Ammonia Borane, *J. Am. Chem. Soc.*, 2009, **131**, 4600–4601; (*b*) A. Meltzer, S. Inoue, C. Präsang and M. Driess, Steering S–H and N–H Bond Activation by a Stable N-Heterocyclic Silylene: Different Addition of H_2S, NH_3, and Organoamines on a Silicon(II) Ligand versus Its $Si(II)\rightarrow Ni(CO)_3$ Complex, *J. Am. Chem. Soc.*, 2010, **132**, 3038–3046; (*c*) D. Wendel, T. Szilvási, D. Henschel, P. J. Altmann, C. Jandl, S. Inoue and B. Rieger, Precise Activation of Ammonia and Carbon Dioixde by an Iminodisilene, *Angew. Chem., Int. Ed.*, 2018, **57**, 14575–14579, (*Angew. Chem.*, 2018, **130**, 14783–14787); (*d*) D. Reiter, P. Frisch, D. Wendel, F. M. Hörmann and S. Inoue, Oxidation reactions of a versatile, two-coordinate, acyclic iminosiloxysilylene, *Dalton Trans.*, 2020, **49**, 7060–7068.

13 Ammonia activation by selected Ge and Sn compounds: (*a*) C. Stanciu, S. S. Hino, M. Stender, A. F. Richards, M. M. Olmstead and P. P. Power, Synthesis and Characterization of Ge(II), Sn(II), and Pb(II) Monoamides with $-NH_2$ Ligands, *Inorg. Chem.*, 2005, **44**, 2774–2780; (*b*) A. Jana, I. Objartel, H. W. Roesky and D. Stalke, Cleavage of a N–H Bond of Ammonia at Room Temperature by a Germylene, *Inorg. Chem.*, 2009, **48**, 798–800; (*c*) W. Wang, S. Inoue, S. Yao and M. Driess, Reactivity of N-Heterocyclic Germylene Toward Ammonia and Water, Reactivity of a N-Heterocyclic Germylene Toward Ammonia and Water, *Organometallics*, 2011, **30**, 6490–6494; (*d*) M. Usher, A. V. Protchenko, A. Rit, J. Campos, E. L. Kolychev, R. Tirfoin and S. Aldridge, A Systematic Study of Structure and E–H Bond Activation Chemistry by Sterically Encumbered Germylene Complexes, *Chem. – Eur. J.*, 2016, **22**, 11685–11698; (*e*) D. C. H. Do, A. V. Protchenko, M. A. Fuentes, J. Hicks, P. Vasko and S. Aldridge, N–H cleavage vs. Werner complex formation: reactivity of cationic group 14 tetrelenes towards amines, *Chem. Commun.*, 2020, **56**, 4684–4687; (*f*) A. C. Phung, J. C. Fettinger and P. P. Power, Insertion Reactions of NH_3 and H_2O with the Ferriogermylenes $ArGeFeCp(CO)_2$ (Ar = Ar^{Me6} ($-C_6H_3$-(C_6H_2-2,4,6-Me_3)$_2$) or Ar^{iPr4} ($-C_6H_3$-(C_6H_3-2,6-$^iPr_2$)$_2$); Cp = η^5-C_5H_5): Structural Isomerism and Polymorphism in a Metallogermylene, *Organometallics*, 2021, **40**, 3472–3479.

14 A. V. Protchenko, J. I. Bates, L. M. A. Saleh, M. P. Blake, A. D. Schwarz, E. L. Kolychev, A. L. Thompson, C. Jones, P. Mountford and S. Aldridge, Enabling and Proving Oxidative Addition and Reductive Elimination at a Group 14 Metal Center: Cleavage and Functionalization of E–H Bonds by a Bis(boryl)stannylene, *J. Am. Chem. Soc.*, 2016, **138**, 4555–4564.

15 Selected review articles on the concept of hemilability: (*a*) A. Bader and E. Lindner, Coordination chemistry and catalysis with hemilabile oxygen-phosphorus ligands, *Coord. Chem. Rev.*, 1991, **108**, 27–110; (*b*) P. Braunstein and F. Naud, Hemilability of Hybrid Ligands and the Coordination Chemistry of Oxazoline-Based Systems, *Angew. Chem., Int. Ed.*, 2001, **40**, 680–699.

16 M. Fischer, M. M. D. Roy, L. L. Wales, M. A. Ellwanger, A. Heilmann and S. Aldridge, Structural Snapshots in Reversible Phosphinidene Transfer: Synthetic, Structural, and Reaction Chemistry of a Sn=P Double Bond, *J. Am. Chem. Soc.*, 2022, **144**, 8908–8913.

17 See the ESI.†

18 (*a*) P. Pyykkö and M. Atsumi, Molecular Single-Bond Covalent Radii for Elements 1–118, *Chem. – Eur. J.*, 2009, **15**, 186–197; (*b*) P. Pyykkö and M. Atsumi, Molecular Double-Bond Covalent Radii for Elements Li–E112, *Chem. – Eur. J.*, 2009, **15**, 12770–12779.

19 The observed P–N bond lengths are in good agreement with other structurally characterized iminophosphoranes, and the following examples show P–N bond lengths from 1.54 Å to 1.60 Å:(*a*) E. Bohm, K. Dehnicke, J. Beck, W. Hiller, J. Strahle, A. Maurer and D. Fenske, Die Kristallstrukturen von Ph_3PNPh, $[Ph_3PN(H)Ph][AuI_2]$ und von 2,3-Bis(triphenylphosphoranimino)maleinsäure-N-methylimid, *Z. Naturforsch., B: J. Chem. Sci.*, 1988, **43**, 138–144; (*b*) A. Müller, M. Möhlen, B. Neumüller, N. Faza, W. Massa and K. Dehnicke, Die Kristallstrukturen der silylierten Phosphanimine $Me_3SiNP(c\text{-}C_6H_{11})_3$ und $(Me_3SiNPPh_2)_2CH_2$, *Z. Anorg. Allg. Chem.*, 1999, **625**, 1748–1751; (*c*) B. Neumüller and K. Dehnicke, Phosphanimin- und Phosphaniminato-Komplexe von Beryllium. Kristallstrukturen von $[BeCl_2(HNPPh_3)_2]$, $[BeCl(HNPPh_3)_2(Py)]Cl$ und $[Be_3Cl_2(NPPh_3)_4]$, *Z. Anorg. Allg. Chem.*, 2004, **630**, 369–376; (*d*) K. E. Aldrich and A. L. Odom, A photochemical route to square planar, ruthenium(IV)-bis(imide), *Chem. Commun.*, 2019, **55**, 4403–4406; (*e*) J. Du, Y. Zhang, Z. Huang, S. Zhou, H. Fang and P. Cui, Heterobimetallic Pd(0) complexes with Pd→Ln (Ln = Sc, Y, Yb, Lu) dative bonds: rare-earth metal-dominated frustrated Lewis pair-like reactivity, *Dalton Trans.*, 2020, **49**, 12311–12318.

20 The P–N bond shortening in iminophosphoranes is due to electrostatics and has been thoroughly investigated: (*a*) M. Bolboaca, T. Stey, A. Murso, D. Stalke and W. Kiefer, P–N Bond Length Alterations Monitored by Infrared Absorption and Fourier Transform Raman Spectroscopy in Combination with Density Functional Theory Calculations, *Appl. Spectrosc.*, 2003, **57**, 970–976; (*b*) N. Kocher, D. Leusser, A. Murso and D. Stalke, Metal Coordination to the Formal P=N Bond of an Iminophosphorane and Charge-Density Evidence against Hypervalent Phosphorus (V), *Chem. – Eur. J.*, 2004, **10**, 3622–3631.

21 S. Freitag, K. M. Krebs, J. Henning, J. Hirdler, H. Schubert and L. Wesemann, Stannylene-Based Lewis Pairs, *Organometallics*, 2013, **32**, 6785–6791.

22 E. D. Glendening, J. K. Badenhoop, A. E. Reed, J. E. Carpenter, J. A. Bohmann, C. M. Morales, P. Karafiloglou, C. R. Landis and F. Weinhold, *NBO 7.0*, Theoretical Chemistry Institute, University of Wisconsin, Madison, WI, 2018.

23 (*a*) Y. Wang and J. Ma, Silylenes and germylenes: The activation of H–H bond in hydrogen molecule, *J. Organomet. Chem.*, 2009, **694**, 2567–2575; (*b*) Y. Peng, B. D. Ellis, X. Wang and P. P. Power, Diarylstannylene Activation of Hydrogen or Ammonia with Arene Elimination, *J. Am. Chem. Soc.*, 2008, **130**, 12268–12269; (*c*) A. V. Protchenko, K. H. Birjkumar, D. Dange, A. D. Schwarz, D. Vidovic, C. Jones, N. Kaltsoyannis, P. Mountford and S. Aldridge, A Stable Two-Coordinate Acyclic Silylene, *J. Am. Chem. Soc.*, 2012, **134**, 6500–6503.

24 D. Bourissou, O. Guerret, F. P. Gabbaï and G. Bertrand, Stable Carbenes, *Chem. Rev.*, 2000, **100**, 39–92.

25 Y. Peng, J.-D. Guo, B. D. Ellis, Z. Zhu, J. C. Fettinger, S. Nagase and P. P. Power, Reaction of Hydrogen or Ammonia with Unsaturated Germanium or Tin Molecules under Ambient Conditions: Oxidative Addition versus Arene Elimination, *J. Am. Chem. Soc.*, 2009, **131**, 16272–16282.

26 J. Abbenseth, O. P. E. Townrow and J. M. Goicoechea, Thermoneutral N–H Bond Activation of Ammonia by a Geometrically Constrained Phosphine, *Angew. Chem., Int. Ed.*, 2021, **60**, 23625–23629, (*Angew. Chem.*, 2021, **133**, 23817–23821).

27 (*a*) S. Bachmann, B. Gernert and D. Stalke, Solution structures of alkali metal cyclopentadienides in THF estimated by ECC-DOSY NMR-spectroscopy (incl. Software), *Chem. Commun.*, 2016, **52**, 12861–12864; (*b*) S. Bachmann, R. Neufeld, M. Dzemski and D. Stalke, New External Calibration Curves (ECCs) for the Estimation of Molecular Weights in Various Common NMR Solvents, *Chem. – Eur. J.*, 2016, **22**, 8462–8465.

28 A. Steiner and D. Stalke, Substituent-Controlled Reactions of Iminophosphoranes with Methyllithium, *Angew. Chem., Int. Ed. Engl.*, 1995, **34**, 1752–1755, (*Angew. Chem.*, 1995, **107**, 1908–1910).

29 T. Ochiai, D. Franz, X.-N. Wu, E. Irran and S. Inoue, A Tin Analogue of Carbenoid: Isolation and Reactivity of a Lithium Bis(imidazolin-2-imino)stannylenoid, *Angew. Chem., Int. Ed.*, 2016, **55**, 6983–6987, (*Angew. Chem.*, 2016, **128**, 7097–7101).

30 D. Reed, D. Stalke and D. S. Wright, Observation of a Direct Sn–Li Bond; The Crystal and Molecular Structure of Monomeric $[Ph_3SnLi{\cdot}PMDETA]$ and the Detection of $^{119,117}Sn$–^{7}Li NMR Coupling in Solution, *Angew. Chem., Int. Ed. Engl.*, 1991, **30**, 1459–1460, (*Angew. Chem.*, 1991, **103**, 1539–1540).

31 (*a*) A. M. Arif, A. H. Cowley and T. M. Elkins, A bulky silyl derivative of tin(II), *J. Organomet. Chem.*, 1987, **325**, C11–C13; (*b*) H. Arp, J. Baumgartner, C. Marschner and T. Müller, A Cyclic Disilylated Stannylene: Synthesis, Dimerization, and Adduct Formation, *J. Am. Chem. Soc.*, 2011, **133**, 5632–5635; (*c*) C. Yan, Z. Li, X. Q. Xiao, N. Wei, Q. Lu and M. Kira, Reversible Stannylenoid Formation from the Corresponding Stannylene and Cesium Fluoride, *Angew. Chem., Int. Ed.*, 2016, **55**, 14784–14787, (*Angew. Chem.*, 2016, **128**, 15004–15007); (*d*) H. Zhao, J. Li, X. Q. Xiao, M. Kira, Z. Li and T. Müller, Cation-Triggered Stannate(II)/Stannylenoid/Stannylene Conversion, *Chem. –*

Eur. J., 2018, **24**, 5967–5973; (*e*) M. Auer, F. Diab, K. Eichele, H. Schubert and L. Wesemann, Reactivity of organogermanium and organotin trihydrides, *Dalton Trans.*, 2022, **51**, 5950–5961; (*f*) X.-X. Zhao, S. Fujimori, J. A. Kelly and S. Inoue, Isolation and Reactivity of Stannylenoids Stabilized by Amido/Imino Ligands, *Chem. – Eur. J.*, 2023, **29**, e202202712.

32 According to IUPAC, carbenoids are defined as "complexed carbene-like entities that display the reactivity characteristics of carbenes, either directly or by acting as sources of carbenes".

33 (*a*) N. Kuhn and T. Kratz, Synthesis of Imidazol-2-ylidenes by Reduction of Imidazole-2(3*H*)-thiones, *Synthesis*, 1993, 561–562; (*b*) C. Barnett, M. L. Cole and J. B. Harper, Steric Properties of *N*-Heterocyclic Carbenes affect the Performance of Electronic Probes, *Eur. J. Inorg. Chem.*, 2021, **47**, 4954–4958.

34 S. K. Chen, W.-Q. Ma, Z.-B. Yan, F.-M. Zhang, S.-H. Wang, Y.-Q. Tu, X.-M. Zhang and J.-M. Tian, Organo-Cation Catalyzed Asymmetric Homo/Heterodialkylation of Bisoxindoles: Construction of Vicinal All-Carbon Quaternary Stereocenters and Total Synthesis of (-)-Chimonanthidine, *J. Am. Chem. Soc.*, 2018, **140**, 10099–10103.

35 (*a*) Y. Liu, J. Du and L. Deng, Synthesis, Structure, and Reactivity of Low-Spin Cobalt(II) Imido Complexes [$(Me_3P)_3Co$ (Nar)], *Inorg. Chem.*, 2017, **56**, 8278–8286; (*b*) K. E. Aldrich and A. L. Odom, A photochemical route to a square planar, ruthenium(IV)-bis(imide), *Chem. Commun.*, 2019, **55**, 4403–4406.

36 Y. M. Badiei, A. Krishnaswamy, M. M. Melzer and T. H. Warren, Transient Terminal Cu-Nitrene Intermediates from Discrete Dicopper Nitrenes, *J. Am. Chem. Soc.*, 2006, **128**, 15056–15057.

37 (*a*) E. Kogut, H. L. Wiencko, L. Zhang, D. E. Cordeau and T. H. Warren, A Terminal Ni(III)-Imide with Diverse Reactivity Pathways, *J. Am. Chem. Soc.*, 2005, **127**, 11248–11249; (*b*) T. F. C. Cruz, L. F. Veiros and P. T. Gomes, Cobalt (I) Complexes of 5-Aryl-2-iminopyrrolyl Ligands: Synthesis, Spin Isomerism, and Application in Catalytic Hydroboration, *Inorg. Chem.*, 2018, **57**, 14671–14685.

38 Bruker AXS Inc., *Bruker Apex CCD, SAINT v8.40B*, Bruker AXS Inst. Inc., Madison, WI, USA, 2019.

39 L. Krause, R. Herbst-Irmer, G. M. Sheldrick and D. Stalke, Comparison of silver and molybdenum microfocus X-ray sources for single-crystal structure determination, *J. Appl. Crystallogr.*, 2015, **48**, 3–10.

40 M. Sevvana, M. Ruf, I. Usón, G. M. Sheldrick and R. Herbst-Irmer, Non-merohedral twinning: from minerals to proteins, *Acta Crystallogr., Sect. D: Struct. Biol.*, 2019, **75**, 1040–1050.

41 G. M. Sheldrick, Crystal structure refinement with *SHELXL*, *Acta Crystallogr., Sect. A: Found. Adv.*, 2015, **71**, 3–8.

42 G. M. Sheldrick, Crystal structure refinement with *SHELXL*, *Acta Crystallogr., Sect. C: Struct. Chem.*, 2015, **71**, 3–8.

43 C. B. Hübschle, G. M. Sheldrick and B. Dittrich, ShelXle: a Qt graphical user interface for *SHELXL*, *J. Appl. Crystallogr.*, 2011, **44**, 1281–1284.

44 M. J. Frisch, G. W. Trucks, H. B. Schlegel, G. E. Scuseria, M. A. Robb, J. R. Cheeseman, G. Scalmani, V. Barone, G. A. Petersson, H. Nakatsuji, X. Li, M. Caricato, A. V. Marenich, J. Bloino, B. G. Janesko, R. Gomperts, B. Mennucci, H. P. Hratchian, J. V. Ortiz, A. F. Izmaylov, J. L. Sonnenberg, D. Williams-Young, F. Ding, F. Lipparini, F. Egidi, J. Goings, B. Peng, A. Petrone, T. Henderson, D. Ranasinghe, V. G. Zakrzewski, J. Gao, N. Rega, G. Zheng, W. Liang, M. Hada, M. Ehara, K. Toyota, R. Fukuda, J. Hasegawa, M. Ishida, T. Nakajima, Y. Honda, O. Kitao, H. Nakai, T. Vreven, K. Throssell, J. A. Montgomery Jr., J. E. Peralta, F. Ogliaro, M. J. Bearpark, J. J. Heyd, E. N. Brothers, K. N. Kudin, V. N. Staroverov, T. A. Keith, R. Kobayashi, J. Normand, K. Raghavachari, A. P. Rendell, J. C. Burant, S. S. Iyengar, J. Tomasi, M. Cossi, J. M. Millam, M. Klene, C. Adamo, R. Cammi, J. W. Ochterski, R. L. Martin, K. Morokuma, O. Farkas, J. B. Foresman and D. J. Fox, *Gaussian 16, Revision A.03*, Gaussian, Inc., Wallingford, CT, 2016.

45 A. D. Becke, Density-functional exchange-energy approximation with correct asymptotic behavior, *Phys. Rev. A*, 1988, **38**, 3098–3100.

46 J. P. Perdew, Density-functional approximation for the correlation energy of the inhomogeneous electron gas, *Phys. Rev. B: Condens. Matter Mater. Phys.*, 1986, **33**, 8822–8824.

47 F. Weigend and R. Ahlrichs, Balanced basis sets of split valence, triple zeta valence and quadruple zeta valence quality for H to Rn: Design and assessment of accuracy, *Phys. Chem. Chem. Phys.*, 2005, **7**, 3297–3305.

48 S. Grimme, J. Antony, S. Ehrlich and H. Krieg, A consistent and accurate *ab initio* parametrization of density functional dispersion correction (DFT-D) for the 94 elements H-Pu, *J. Chem. Phys.*, 2010, **132**, 154104.

49 S. Grimme, S. Ehrlich and L. Goerigk, Effect of the damping function in dispersion corrected density functional theory, *J. Comput. Chem.*, 2011, **32**, 1456–1465.